Cell

# *C. elegans* Telomeres Contain G-Strand and C-Strand Overhangs that Are Bound by Distinct Proteins

Marcela Raices,[1] Ramiro E. Verdun,[1] Sarah A. Compton,[2] Candy I. Haggblom,[1] Jack D. Griffith,[2] Andrew Dillin,[1] and Jan Karlseder[1,*]
[1]The Salk Institute for Biological Studies, 10010 North Torrey Pines Road., La Jolla, CA 92037, USA
[2]Lineberger Comprehensive Cancer Center, University of North Carolina School of Medicine, Mason Farm Road, Chapel Hill, NC 27599, USA
*Correspondence: karlseder@salk.edu
DOI 10.1016/j.cell.2007.12.039

## SUMMARY

Single-strand extensions of the G strand of telomeres are known to be critical for chromosome-end protection and length regulation. Here, we report that in *C. elegans*, chromosome termini possess 3′ G-strand overhangs as well as 5′ C-strand overhangs. C tails are as abundant as G tails and are generated by a well-regulated process. These two classes of overhangs are bound by two single-stranded DNA binding proteins, CeOB1 and CeOB2, which exhibit specificity for G-rich or C-rich telomeric DNA. Strains of worms deleted for CeOB1 have elongated telomeres as well as extended G tails, whereas CeOB2 deficiency leads to telomere-length heterogeneity. Both CeOB1 and CeOB2 contain OB (oligo-saccharide/oligo-nucleotide binding) folds, which exhibit structural similarity to the second and first OB folds of the mammalian telomere binding protein hPOT1, respectively. Our results suggest that *C. elegans* telomere homeostasis relies on a novel mechanism that involves 5′ and 3′ single-stranded termini.

## INTRODUCTION

Telomeric 3′ overhangs have been observed in many model organisms, including yeast, ciliates, trypanosomes, plants, mice, and humans (Hemann and Greider, 1999; Jacob et al., 2003; Makarov et al., 1997; McElligott and Wellinger, 1997; Riha et al., 2000; Wellinger et al., 1993; Wright et al., 1997). Chromosome end replication in ciliates and *S. cerevisiae* involves the coregulated activities of telomerase and fill-in synthesis by the lagging strand machinery (Bianchi et al., 2004; Chandra et al., 2001; Diede and Gottschling, 1999; Fan and Price, 1997; Pennock et al., 2001). Similarly, studies in mammalian systems have proposed that telomerase-dependent elongation of the G strand is coordinated with C strand synthesis (Nakamura et al., 2005). However, G-tails have been observed in the absence of telomerase activity (Dionne and Wellinger, 1996; Hemann and Greider, 1999; Nikaido et al., 1999), suggesting that overhangs are generated by an active processing mechanism following telomere replication and not by telomerase-mediated elongation of the G strand.

The knowledge of the molecular mechanism of overhang generation remains incomplete. Lagging-strand synthesis results in a short 3′ overhang at the chromosome terminus, resulting from removal of the most distal RNA primer utilized for Okazaki fragment synthesis. Leading-strand synthesis is expected to generate a blunt end. However, both telomere termini end in single-stranded G overhangs that are much longer than the RNA primers in yeast, ciliates, and humans, indicating a well-regulated processing of chromosome ends (Chai et al., 2006; Jacob et al., 2001; Makarov et al., 1997; Wellinger et al., 1996). It is likely that G tails are generated by enzymatic resection of the telomeric C strand, but the nucleases responsible have not been described. It is also unclear if the telomeric leading and lagging strands are differentially synthesized at discrete stages in the cell cycle, and how telomerase participates in this complex process.

Proteins specialized to bind to the single-stranded 3′ overhang and to promote chromosome-end protection have been described in a variety of model systems. In *S. cerevisiae*, Cdc13p plays a role in telomerase recruitment, but loss of Cdc13p leads to extensive degradation of the telomeric C strand and the generation of long G overhangs, triggering cell-cycle arrest (Booth et al., 2001; Garvik et al., 1995; Grandin et al., 2001, 1997). *S. pombe* lacking the single-stranded binding factor POT1 rapidly lose telomeric DNA, but some cells survive by circularizing their chromosomes (Baumann and Cech, 2001). In mice, POT1b loss leads to degradation of the C strand, suggesting a protective mechanism analogous to Cdc13 in yeast (Hockemeyer et al., 2006). Loss of the telomeric G-tail has also been observed in the absence of the telomeric protection factor TRF2 from chromosome ends, indicating that the shelterin complex together with the telomeric double-stranded and single-stranded DNA forms a protective unit at telomeres (de Lange, 2005).

Telomeric overhangs have also been predicted to play a prominent role in formation of loops at chromosome ends, when it was observed that a fraction of telomeres form lasso-like structures by invasion of the single strand into the double-stranded

homologous telomeric DNA (Griffith et al., 1999). Loops have been found in a wide variety of systems (de Lange, 2004), raising the possibility that they are a commonly employed mechanism for protecting telomeres from recognition as double-stranded breaks.

The telomeres of the nematode *C. elegans* are 2–9 kb in length and consist of the repeated DNA sequence TTAGGC. It is known that telomere length in the worm is clonal, inherited, and regulated *in cis* (Raices et al., 2005), similar to telomere length in mammalian cells. However, no homologs of the mammalian telomeric binding proteins TRF1, TRF2, TPP1, TIN2, or POT1 have been described so far, and were not readily visible in the completed *C. elegans* genome. A candidate for the catalytic subunit of telomerase has been identified, and its deletion causes gradual telomere shortening, leading to chromosome fusion, loss of viability, and infertility (Meier et al., 2006). Telomere length in *C. elegans* strains has also been analyzed by STELA (single telomere length analysis), a PCR-based method for estimating the length of individual telomeres. Application of this method in *C. elegans* revealed that the C-rich strand ends preferentially in TCC-5′ (Cheung et al., 2004).

Here, we analyzed *C. elegans* telomeric structure in detail and found that worms not only contain 3′ G-rich overhangs, but also 5′ C-rich tails. Two-dimensional gel analysis and electron microscopy revealed the presence of telomeric circles and telomeric loops. We identified two OB-fold-containing proteins with similarity to hPOT1 that bind to either the G-rich or the C-rich nematode telomeric sequence, and whose deletions lead to changes in telomere length, heterogeneity, and accumulation of telomeric circles. We therefore propose that *C. elegans* employs on a novel mechanism for telomere homeostasis that incorporates 5′ and 3′ overhangs.

## RESULTS

### *C. elegans* Chromosomes Terminate with Either 3′ G Tails or 5′ C Tails

To analyze single-strand overhangs at nematode telomeres, genomic DNA was isolated and digested as described (Raices et al., 2005), and subjected to nondenaturing gel electrophoresis (Hemann and Greider, 1999). The dried gels were hybridized with a probe complementary to the G overhang [$(GCCTAA)_4$], and with a probe complementary to the C strand [$(TTAGGC)_4$] as control. DNA from five different wild-type worm strains was loaded alongside DNA from transformed human cancer cells (HeLa) and primary human fibroblasts (IMR90). Exposure of the dried gels revealed strong signals resulting from single-stranded G tails (Figure 1A). The signal stretched from the 9.4 kb marker to the bottom of the gel, with a strong signal in the low molecular weight range. Telomeres in nematodes range from 2–9 kb, suggesting that the higher molecular weight signal results from overhangs at telomeres, and the lower molecular weight signal from a different population of single-stranded TTAGGC-containing molecules (Figure 1A). The nature of these molecules is currently under investigation, and they can be separated from telomeric DNA by 2D electrophoresis, as described in Figure 2. The DNA from the human cell lines crosshybridized with the *C. elegans* telomeric probes, resulting in a signal in the lanes loaded with HeLa or IMR90 DNA (Figure 1A). When the same DNA was hybridized with oligonucleotides complementary to the C strand, no signal was visible in the lanes loaded with human DNA, but a strong signal was observed in all *C. elegans* DNA lanes (Figure 1B). Denaturation of the gels and subsequent hybridization with the same probes resulted in identical telomeric smear signals for both the G- and the C-rich oligonucleotides in the expected size range from 2–9 kb, interspersed by sharper bands, resulting from intrachromosomal telomeric repeats (Figures 1A and 1B). Taken together, it appears that *C. elegans* contains both G- and C-rich overhangs.

The signal resulting from hybridization with the G-rich probe was unexpected, since this usually serves as a negative control, and does not lead to hybridization. To exclude the possibility that G-rich probe signals result from accessibility of hybridization probes to double-stranded regions of nematode DNA, we tested whether the signal resulted from terminal DNA fragments. Bal-31 digestion of genomic DNA degrades the DNA from the ends, and has frequently been used to confirm that hybridization signals result from terminal DNA. Digests of nematode DNA with Bal-31 nuclease resulted in rapid loss of the overhang signal. After 5 min of Bal-31 digestion almost no signal could be detected by hybridization of native gels, and after 20 min of digestion the signal was undetectable (Figures S1A and S1B available online). It required 120 min of Bal-31 incubation to remove the bulk of double-stranded telomeric DNA, as visualized by hybridization of denatured gels (Figures S1A and S1B). Bal-31 is not strand specific, and both the signals resulting from hybridization with C-rich probes and G-rich probes were removed with the same efficiency (Figures S1A and S1B). Mung bean nuclease digests single-stranded DNA at termini and in DNA loops. Similarly to Bal-31 digests, a short incubation with the nuclease resulted in loss of the signal resulting from the C- and the G-rich probes, whereas the double-stranded DNA remained undigested (Figures S1C and S1D). However, since Mung bean nuclease and Bal-31 are both capable of digesting intrachromosomal single-stranded DNA (Gray et al., 1975; Gubler, 1987), we performed Exonuclease 1 digests. Exonuclease 1 degrades terminal DNA in 3′ to 5′ direction, effectively removing 3′ telomeric G tails (Hemann and Greider, 1999). Digestion of *C. elegans*, IMR90 or HeLa DNA with this enzyme resulted in efficient loss of the G strand signal, as visualized by hybridization of native gels with a probe complementary to the G overhang (Figures 1C and 1E). Hybridization of the same gels with the same probe after denaturation demonstrated that the double-stranded DNA was still intact (Figure 1C). These results suggest that the signal resulted from terminal G-rich 3′ overhangs, establishing firmly that nematode telomeres end in G tails. However, Exonuclease 1 had no effect on the signal resulting from hybridization with a telomeric G probe in native or denatured conditions (Figures 1D and 1E), confirming the possibility that this signal might be due to 5′ telomeric C-rich overhangs at *C. elegans* chromosome ends. We noted that the undefined single-stranded repeats at the bottom of the gels were only partially sensitive to Exonuclease 1 which could be due to the formation of secondary structures, however, at this point we lack an explanation for this phenomenon.

To better separate the telomeres from the single-stranded fragments, we established 2D gel electrophoresis for *C. elegans*

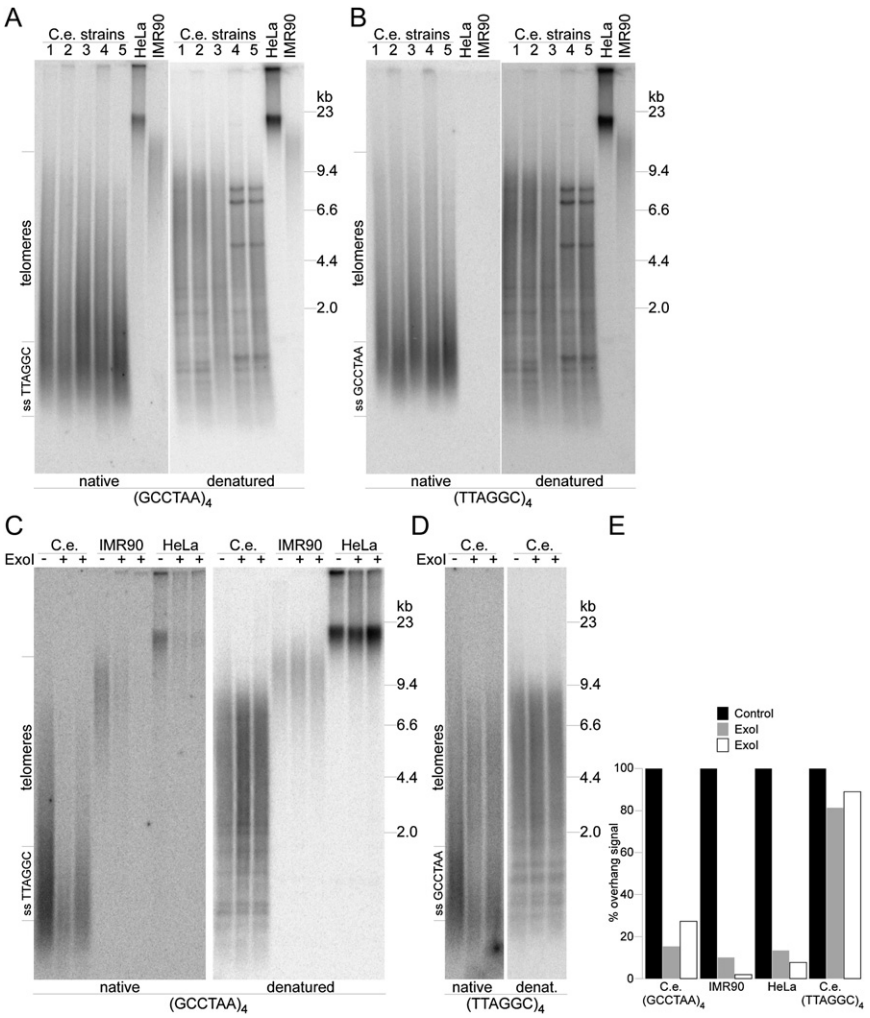


**Figure 1. *C. elegans* Telomeres Have 3′ G Tails and 5′ C Tails**

(A) Southern analysis of *C. elegans* telomeres under native (left panel) and denatured (right panel) conditions. DNA from five different strains (N2, N2 ancestral, CF512, CB3191, and CB3192) of HeLa cells and IMR90 fibroblasts was digested and separated by agarose gel electrophoresis as described (Karlseder et al., 2002; Raices et al., 2005). The gels were dried and hybridized with a radioactively labeled $(GCCTAA)_4$ oligonucleotide complementary to the nematode telomeric G strand. Telomeres, single-stranded telomeric DNA, and fragment size are indicated.

(B) As in (A), except that the gels were hybridized with a radioactively labeled $(TTAGGC)_4$ oligonucleotide complementary to the telomeric C strand.

(C) Exonuclease 1 digestion of DNA extracted from wild-type *C. elegans*, IMR90, and HeLa cells. The DNA was separated by agarose gel electrophoresis and hybridized with radioactively labeled $(GCCTAA)_4$ probes complementary to the telomeric G strand under native (left panel) and denatured (right panel) conditions. Telomeres, single-stranded telomeric DNA, and fragment size are indicated.

(D) As in (C) for *C. elegans* DNA, except that the gels were hybridized with a radioactively labeled $(TTAGGC)_4$ oligonucleotide complementary to the telomeric C strand.

(E) Quantification of (C) and (D).

telomeres. DNA from *C. elegans*, IMR90 primary fibroblasts and KMST-6 human ALT cells was separated by size on the x axis and by conformation on the y axis (Cesare and Griffith, 2004) (Figure 2A) and hybridized with C and G probes under native and denaturing conditions. Hybridization of native 2D gels loaded with nematode DNA with a $(GCCTAA)_4$ probe resulted in a strong signal of the telomeric G overhangs (blue arrows) that was well-separated from the low molecular weight single-stranded G-rich DNA (green arrows) (Figure 2B, upper first panel). Hybridization of native 2D gels loaded with DNA isolated from KMST-6 ALT cells with a $(CCCTAA)_4$ probe resulted in a similar pattern, displaying telomeric overhangs (blue arrows) and single-stranded low molecular weight G-rich DNA (green arrows) (Figure 2B, upper second panel). Only the G overhang arc was observed in IMR90 DNA (Figure 2B, upper third panel). When the DNA in the gels was denatured and rehybridized with the same probes, *C. elegans* telomeres arranged in a telomeric arc, but also displayed a second arc above the telomeric fragments (Figure 2B, lower first panel, red arrows), characteristic of telomeric circles, which were also observed in ALT cells (Figure 2B, lower second panel, red arrows) (Cesare and Griffith, 2004; Wang et al., 2004), but absent in IMR90 cells (Figure 2B, lower third panel). When 2D gels with DNA from worms and human cells were analyzed with probes complementary to the C strand, only hybridization of *C. elegans* DNA resulted in a signal under native conditions (Figure 2C, upper panel). Again, the telomeric signal (blue arrow) was distinct from the single-stranded fragments (green arrow). Denaturation and rehybridization of the DNA in the gels generated strong telomeric signals in all three DNA samples, and the additional arcs (red arrows) resulting from telomeric circles were clearly visible in worm DNA and DNA from ALT cells (Figure 2C, lower panels).

Since the 2D gel analysis allowed efficient separation of telomeric fragments from low molecular weight DNA, we analyzed the effects of Exonuclease 1, which specifically degrades 3′ single-stranded overhangs, and of $RecJ_f$, an exonuclease that specifically degrades 5′ single-stranded overhangs (Lovett and Kolodner, 1989). Analysis of worm DNA under native and denaturing conditions revealed again that Exonuclease 1 efficiently removed the 3′ G overhangs. When hybridized under native conditions with a C-rich probe, the telomeric arc signal was undetectable after Exonuclease 1 digestion (Figure 2D, upper left two panels). Denaturation of the gels demonstrated that the genomic DNA was not degraded and telomeres were still readily detectable (Figure 2D, lower left two panels). In contrast, incubation with Exonuclease 1 did not change the signal intensity resulting from hybridization with a probe complementary to the C strand under native or denaturing conditions (Figure 2D, right

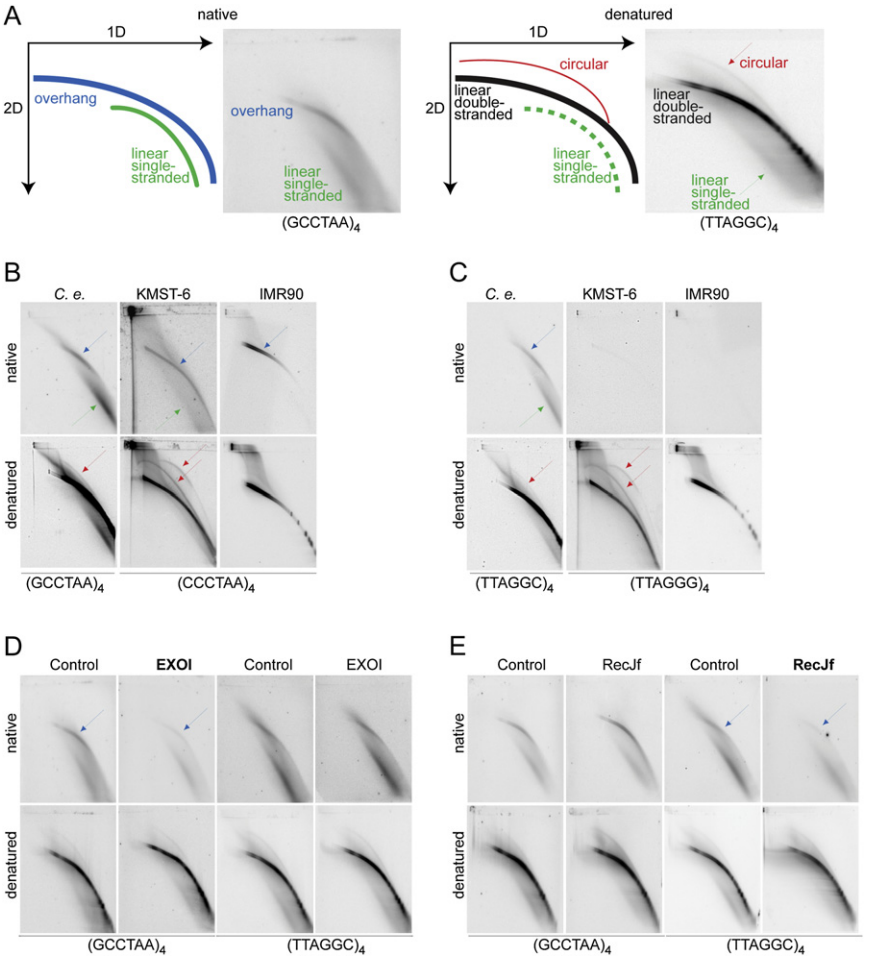


**Figure 2. Two-Dimensional Analysis of *C. elegans* Telomeres**

(A) Schematics and examples of native (left) and denatured (right) 2D gels, indicating the telomeric single-stranded overhangs (blue), single-stranded DNA (green), telomeric arc (black), and circular telomeric DNA (red).

(B) Native and denatured 2D gels of *C. elegans* DNA (*C. e.*), ALT cell DNA (KMST-6) and IMR90 DNA, hybridized with radioactively labeled $(GCCTAA)_4$ and $(CCCTAA)_4$ oligonucleotides, respectively.

(C) As in (B), except that the gels were hybridized with radioactively labeled $(TTAGGC)_4$ and $(TTAGGG)_4$ oligonucleotides, respectively.

(D) 2D gels of *C. elegans* DNA under native and denatured conditions. In the Exonuclease 1 lanes, the DNA was subjected to digestion with Exonuclease 1 (3′ to 5′ polarity) prior to separation. The gels were hybridized with radioactively labeled $(GCCTAA)_4$ and $(TTAGGC)_4$ oligonucleotides as indicated.

(E) As in (D), except that the DNA was digested with the 5′ to 3′ exonuclease $RecJ_f$ as indicated.

two panels). The situation was reversed when the DNA was digested with $RecJ_f$. G overhang analysis demonstrated that 3′ G tails were unaffected by $RecJ_f$ under native conditions (Figure 2E, left two panels). In contrast, $RecJ_f$ efficiently removed 5′ C overhangs from worm chromosome ends, as demonstrated by the complete loss of signal after hybridization with a $(TTAGGC)_4$ probe under native conditions (Figure 2F, upper right two panels). Like Exonuclease 1, $RecJ_f$ did not degrade double-stranded genomic DNA (Figure 2F, lower right two panels). Taken together, these results suggest that *C. elegans* telomeres contain 3′ G tails and 5′ C tails on their chromosome ends.

## The Recessed G Strand Present at Overhangs Preferentially Ends in TTA-3′

In both human cells and in worms, the recessed C strand present at termini with G tails ends preferentially at a specific sequence (Cheung et al., 2004; Sfeir et al., 2005), suggesting a well-regulated generation of the 3′ G-rich overhang. To ask whether C-tail formation in *C. elegans* is also a regulated process, we developed an inverted STELA method, dependent on the presence of 5′ C overhangs, and capable of amplifying telomeric fragments from both arms of *C. elegans* chromosome V (Figure 3A). An inverted telorette is ligated to the 3′ end of the G-rich strand, followed by amplification of a telomeric fragment with a teltail primer complementary to the inverted telorette, and a specific primer complementary to the subtelomeric region of either the left or the right arm of chromosome V (Figure 3A).

When this method was applied to DNA from worm strains with either short telomeres (Figures 3B and 3C, N2 strains) or long telomeres (Figures 3B and 3C, CC2 strain), telomeric products with the expected length could be amplified on both chromosome arms with STELA and inverted STELA (Figure 3B for chromosome VL, Figure 3C for VR). STELA was performed with the optimized telorette 503 (Cheung et al., 2004), and the amplification/hybridization protocol yielded strong signals (Figures 3B and 3C), in accord with previous observations. The inverse STELA protocol was also capable of amplifying telomeric fragments of the expected size with primers, whose binding is dependent on the presence of a 5′ C-rich overhang. However, signal intensities were much weaker and less bands appeared (Figure 3B, C). This raised the possibility that the inverted telorette 503 (INV-1) is capable of being ligated to the end of the G strand at only a small fraction of telomeres. We therefore tested all permutations of the inverted telorette (INV-2 to 6, Figure 3A), and found that INV-4, ending in 5′-GCCTAA-3′, was by far the most efficient for amplification of telomeric fragments (Figures 3D and 3E). Weak amplification was observed with INV- 1 and 6, and no amplification was possible with INV-2, 3, 5, when an only unrelated linker, the teltail oligo, or no linker was added. Amplification was dependent on the addition of *C. elegans* DNA and Ligase. PCR requirements for the left or the right arm of chromosome V were identical (Figures 3D and 3E). These controls suggest that the amplified fragments are not primer multimers (unrelated linker, teltail only, no linker, unrelated

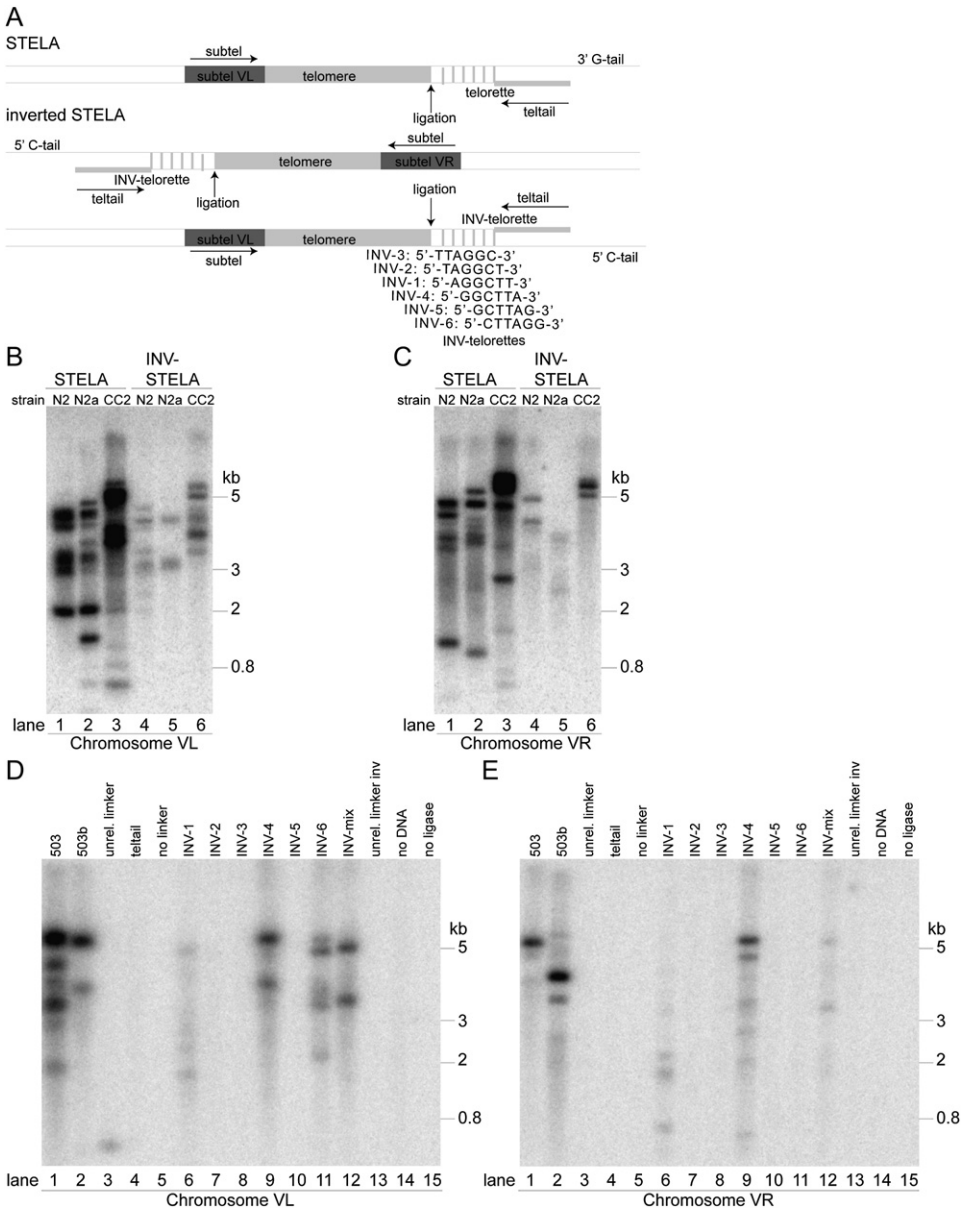


**Figure 3. *C. elegans* 5′ C Tails End Preferentially in TTA-5′**

(A) Schematic of STELA and inverted STELA (INV-STELA). The subtelomeric primers (subtlel), telorettes, inverted telorettes (INV-telorettes), and teltail have been indicated. All six permutations of the inverted telorette are listed.

(B) STELA and inverted STELA for DNA from three *C. elegans* strains with different telomere length. Lanes 1, 2, 4, and 5 represent DNA from N2 strains with short telomeres (N2, N2a [ancestral]), and lanes 3 and 6 DNA from strain CC2 with long telomeres. The PCR reactions were performed with subtelomeric primers specific for the left arm of chromosome V (VL). Fragment size is indicated in kb.

(C) As in (B), except that subtelomeric primers specific for the right arm of chromosome V have been used (VR).

(D) STELA (lanes 1 and 2) and inverted STELA (lanes 3 to 15) of *C. elegans* DNA using subtelomeric primers specific for the left arm of chromosome V (VL). 503 and 503b: Optimized STELA telorette (Cheung et al., 2004); unrel. Linker, template ligated to unrelated telorette; teltail, template ligated to the telomeric primer alone; no linker, PCR reaction without telorette; INV-1 to INV-6, Ligation with all permutations of the inverted telorette, as listed in (A); INV-mix, Ligation with a mix of all six permutations of telorette; unrel. Linker inv, Ligation with inverted unrelated telorette; no DNA, Reaction without addition of *C. elegans* DNA; no Ligase, No Ligase added during the ligation step. Fragment size has been indicated in kb.

(E) as in (D), except that subtelomeric primers specific for the right arm of chromosome V were used (VR).

inverted linker and no DNA controls). Moreover, the requirement for ligase emphasizes that the C overhangs are terminal, and amplification does not result from C-teltail primers binding to partially denatured DNA. Finally, the increased amplification efficiency upon ligation of INV-telorette 4 suggests that the recessed telomeric G strand at 5′ C tails frequently ends in

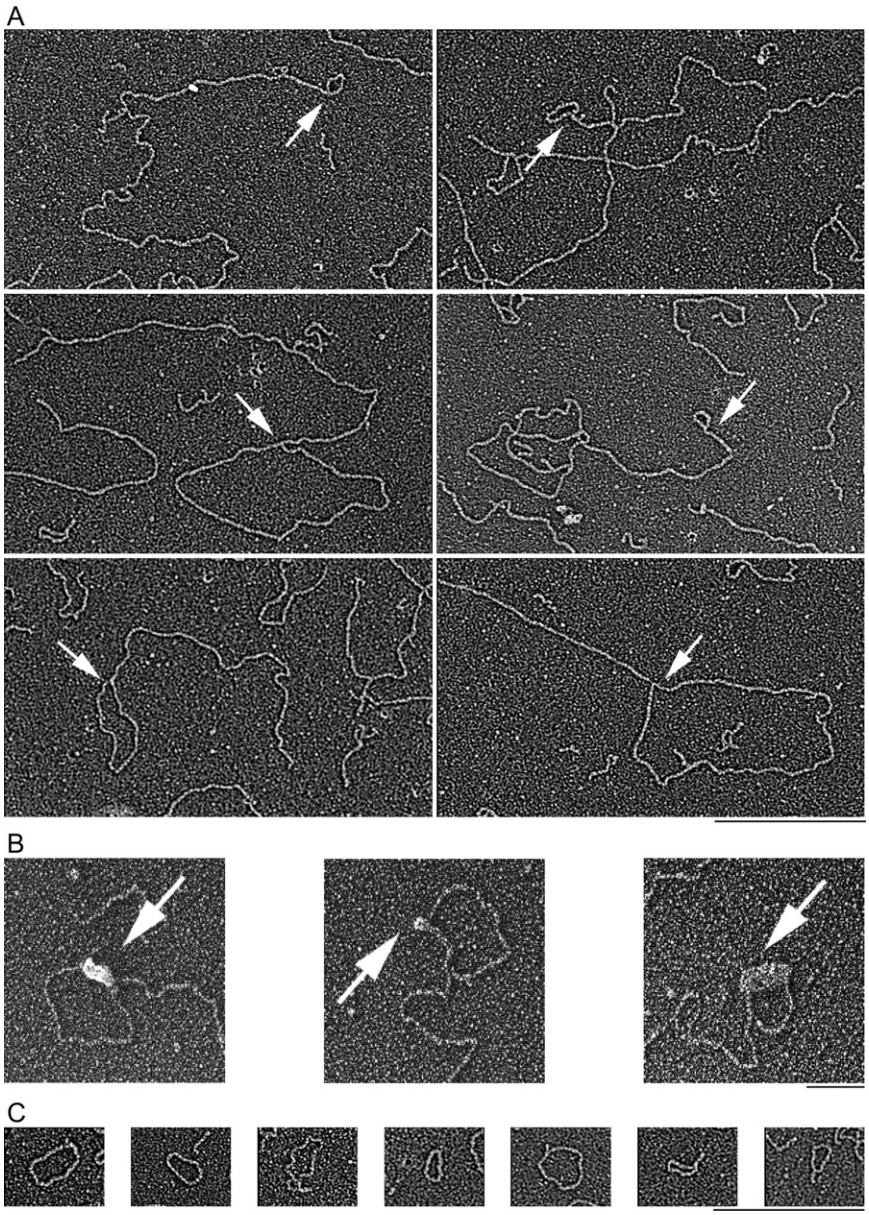


**Figure 4. *C. elegans* Form T Loops and Contain T Circles**

(A) DNA was prepared by surface spreading with cytochrome C followed by rotary shadowcasting with platinum-paladium. Examples of t loops isolated from *C. elegans* chromosomes shown in reverse contrast. Arrows indicate the loops. The scale bar represents 1.0 μM.

(B) DNA was incubated with single-stranded binding protein and the resulting protein-DNA complexes adsorbed onto carbon EM supports followed by rotary shadowcasting with tungsten images demonstrate single-stranded binding protein bound to the base of the t loops. Protein accumulations are indicated by arrows. Bar is equivalent to 50 nM.

(C) Examples of T circles isolated from *C. elegans* and mounted for EM by surface spreading. The scale bar represents 1.0 μM.

TTA-3′, suggesting a well regulated mechanism for generation of 5′ overhangs.

## T Loops and T Circles in *C. elegans*

It has been proposed that the single-stranded telomeric G overhang is capable of invading the homologous double-stranded DNA, forming a lasso-like structure termed telomeric loop or t loop (Griffith et al., 1999). The discovery that *C. elegans* telomeres contain long single-stranded overhangs prompted us to perform electron-microscopic analysis (EM) of worm telomeres. To separate genomic DNA from telomeric DNA we took advantage of the wild-type CC2 strain, which contains telomeres up to 12kb in length (Raices et al., 2005), allowing size exclusion chromatography to enrich for telomeric fragments (Griffith et al., 1999). EM analysis of the fractions enriched for telomeres revealed the lasso like structures characteristic for t loops (Figure 4A). Single-stranded binding protein (SSB) was observed at the base of the loop at the putative invasion site of the single-stranded overhang into double-stranded telomeric tracts (Figure 4B). The amount of bound SSB was variable, likely due to differences in SSB binding efficiency and length of the overhang.

Comparison between non crosslinked and cross linked DNA fractions revealed on average 3% of looped molecules without the addition of psoralen, and 15% loops after psoralen treatment (Table S1), suggesting that the loops are stabilized by crosslinking T residues on opposite strands.

Measurement of loop sizes revealed that 89.3% loops were in the size range of 1–3 kb (50 of 56), 5.4% in the range of 3–6 kb (3 of 56), and 5.4% above 6 kb (3 of 56) (Figure S2A). Loop size in mammals was random, restricted only by the length of telomeric tracts (Griffith et al., 1999), however, there appears to exist a tendency for smaller loop sizes in *C. elegans*, since the mean loop was found to be 1.7 kb in length at a telomere length of 10–12 kb (Figure S2A). We observed that 68% of the tails investigated were below 9 kb in length, but occasionally tails up to 20 kb in length were present, potentially resulting from incomplete digestion of genomic DNA (Figure S2B).

EM analysis of worm telomeres also revealed the presence of t circles (Figure 4C). T circles contained double-stranded telomeric DNA, since they were susceptible to digestion with DdeI, a restriction enzyme that cuts in the nematode telomeric sequence (data not shown). T circles have previously been observed in ALT cells (Cesare and Griffith, 2004; Wang et al.,

2004), where 58% of circles were found in the size range below 6 kb, suggesting that circle size distribution was skewed toward smaller molecule sizes. The circles found in *C. elegans* also had the tendency to be small molecules, since 67% of circles analyzed (16 of 24) were in the size range below 2 kb (Figure S2C).

In summary, *C. elegans* telomeres were found to be capable of t loop formation, but loop size was skewed toward small circles. T circles, previously detected in ALT cells, were also found in worms.

### *C. elegans* Has Two OB-Fold-Containing Proteins with Specificity for G-Rich and C-Rich Single-Stranded DNA

The single-stranded G-rich telomeric overhangs in ciliates, yeast and mammals are recognized by proteins containing OB folds (Theobald and Wuttke, 2004).

By comparing *C. elegans* proteins to a database of known protein structures, hPOT1 and TEBP$\alpha$ were found to display significant structural homology to four proteins (Table S2). Deletion mutants for 3R5.1 did not exhibit a telomeric phenotype, and F39H2.5 deletion displayed a generation dependent progressive telomere shortening phenotype, which is not compatible with a POT1 like phenotype (data not shown). Consequently we focused on a 33 kD and a 40 kD protein, which we named CeOB1 and CeOB2. CeOB1 has similarity to the second OB fold of hPOT1 and TEBP$\alpha$, whereas CeOB2 displays similarity to the first OB fold (Figure 5A). Amino acid alignment revealed 23% and 20% identity between CeOB1, CeOB2 and POT1, respectively (Figure S3A). Structure predictions for CeOB1 and CeOB2 (Figures S3B and S3C) revealed high degree of structural alignment for CeOB1, CeOB2 and hPOT1 in the OB fold containing domain (Figure 5B, Table S3, and Figures S3B and S3C).

To test the DNA binding properties of CeOB1 and CeOB2 we expressed the proteins as $His_9$ tag fusions in bacteria, and purified them (Figure 5C). CeOB1 was soluble and highly expressed, and purified as a single band, whereas CeOB2 displayed lower expression levels and solubility and was less stable (Figure 5C). Gel shift analysis revealed that CeOB1 had no affinity for the telomeric C strand, since it did not bind a $(GCCTAA)_3$ oligonucleotide in a gel retardation assay (Figure 5D, lanes 2 to 4). However, CeOB1 bound to the nematode G-rich telomeric sequence (Figure 5D, lanes 7–9). The absence of protein did not result in a shift of the oligo (lanes 1, 5, 10), and neither did an unrelated protein (GST, lanes 6, 11). CeOB1 also did not bind to a non related sequence with the same GC content as the telomeric G probe (lanes 12–14), suggesting that the protein binds specifically to the nematode telomeric G-rich single strand.

CeOB2 displayed specific affinity to the single-stranded telomeric C strand (Figure 5E, lanes 2 and 3), but did not bind to the G strand or to an unrelated oligonucleotide with the same GC content as the telomeric C probe (Figure 5E, lanes 5, 6, 8, and 9). The band appearing in lanes 7–9 is not protein specific, since it also appears when no protein was added. Next we established the minimal repeat number for binding, and we determined the $K_D$ values for binding of CeOB1 and CeOB2. CeOB1 required at least two TTAGGC repeats for binding, whereas CeOB2 bound stably to a single GCCTAA repeat. The $K_D$ values for the proteins were in 15nM for CeOB1 and 90nM for CeOB2 (Table S4), which is comparable to other OB fold containing telomeric proteins (Anderson et al., 2002; Lei et al., 2002; Nugent et al., 1996).

To confirm that the bands in the gelshift resulted from specific binding of the bacterially expressed proteins we performed supershifts with antibodies against the N-terminal $His_9$ tag on CeOB1 and CeOB2. Increasing amounts of IgG did not result in additional higher molecular weight bands, but a specific anti-His antibody readily shifted the CeOB1 and CeOB2-DNA complexes, suggesting that the bands result from the purified proteins (Figure 5F). Specificity was confirmed when addition of increasing amounts of non radioactively labeled $(TTAGGC)_3$ nucleotides led to a strong reduction in binding of CeOB1 (Figure 5G) and addition of $(GCCTAA)_3$ oligos led to a strong reduction in binding of CeOB2 (Figure 5H). Oligonucleotides of unrelated sequence were not capable of competition (Figures 5G and 5H).

To test the preferred polarity of CeOB1 binding, we performed mobility shift assays with oligonucleotides that carry 12 bases of nontelomeric sequence with the same GC content as *C. elegans* telomeres, followed by 3 TTAGGC repeats at the 3′ end (NR-$(TTAGGC)_3$-3′), or oligos that carried 3 TTAGGC repeats at the 5′ end, followed by 12 bases of nontelomeric sequence (5′-$(TTAGGC)_3$-NR). CeOB1 displayed strong binding when the telomeric repeats were at the 3′ end of the fragment, but no binding when the repeats were at the 5′ end, suggesting that CeOB1 requires a 3′ single-stranded telomeric overhang (Figure 5I, left panel).

CeOB2 was less selective and could bind to the C-rich telomeric sequence when it was 5′ terminal (5′-$(GCCTAA)_3$-NR), or not (NR-$(GCCTAA)_3$-3′) (Figure 5I, right panel), suggesting that CeOB2 can bind to single-stranded C-rich telomeric repeat without preference of an end.

In summary, these results suggest that nematodes encode at least two OB fold containing proteins with homology to the OB folds of TEBP$\alpha$/POT1. CeOB1 specifically binds to the end of the telomeric G overhang, whereas CeOB2 prefers the telomeric C-rich single strand as substrate.

### CeOB1 and CeOB2 Localize to Telomeres

To test whether CeOB1 and CeOB2 can bind to the base of the T loops in EM studies, we incubated purified His-tagged proteins with DNA fractions containing loops. SSB was again used as a positive control, and bound to the loop junctions as described earlier (Figures 4B and 6A). Similarly to SSB, both nematode proteins were found at the invasion site of the single-stranded overhangs into the double-stranded telomeric tracts (Figure 6A). However, the finding that both nematode proteins can bind to the base of telomeric loops only suggests the presence of single-stranded G- and C-rich DNA, and is not prove of t loop formation by invasion of a 3′ or 5′ overhang into complementary sequences. The nonrelated protein GST was used as a negative control and did not display any binding (data not shown).

To test whether CeOB1 and CeOB2 can be crosslinked to telomeric DNA we performed chromatin immunoprecipitations. We generated transgenic worms expressing HA tagged CeOB1 and CeOB2 under control of the *pha-4* promoter (Panowski et al., 2007). Expression was verified by western analysis with

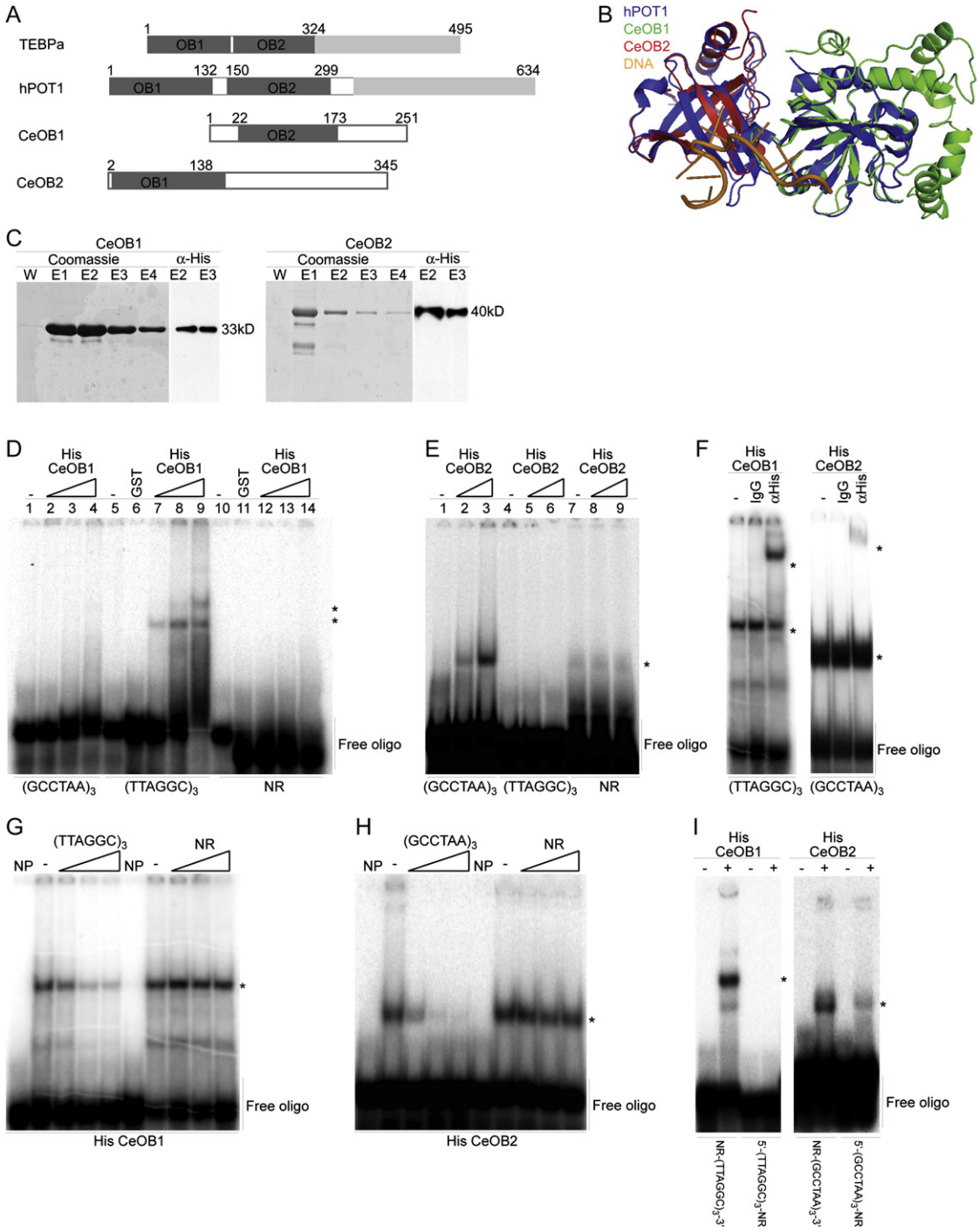


**Figure 5. *C. elegans* Contains Two OB-Fold-Containing Proteins that Bind to G and C Single-Strand DNA Substrates**

(A) Schematic representation of TEBP$\alpha$, hPOT1, CeOB1 and CeOB2 domain organization. Numbers indicate amino acids.

(B) Predicted 3D alignment of POT1 (blue) with CeOB1 (green) and CeOB2 (red); DNA (orange). For details, see Experimental Procedures.

(C) Purification of CeOB1 (left panel) and CeOB2 (right panel). The wash (W) and elution fractions 1 to 4 (E1 to E4) are shown for the Coomassie stained gels, and elution fractions E2 and E3 for western analysis using anti-His antibodies.

(D) Radioactively labeled oligos $(GCCTAA)_3$, $(TTAGGC)_3$, or an unrelated sequence (NR) with the same GC content as the nematode G strand (200 nM) were incubated in the presence of either no protein (- lanes), GST alone (GST lanes), or increasing amounts of purified His-CeOB1 (25–50–100 nM final concentration). Signals resulting from the free oligos are indicated, and the asterisks show the bands resulting from addition of CeOB1.

(E) As in (C), except that the reactions were performed with His-CeOB2.

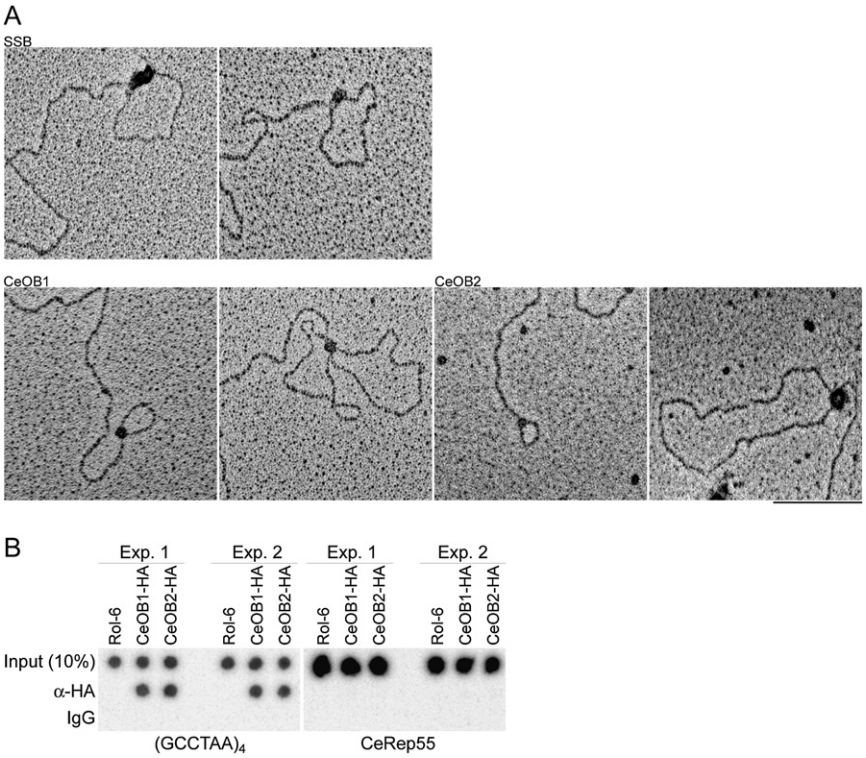


**Figure 6. CeOB1 and CeOB2 Bind to Telomeres**

(A) Electron microscopy of CeOB1 and CeOB2 bound to t loop-containing fractions. Single-stranded binding protein SSB, CeOB1, and CeOB2 were incubated with purified telomeric DNA fractions and mounted for EM. Two examples of SSB, CeOB1, and CeOB2 bound to the single-stranded DNA at the base of the t loop junction are shown. The scale bar represents 100 nM.

(B) Chromatin immunoprecipitations of HA-tagged CeOB1 and CeOB2. Precipitations were carried out with anti-HA antibodies (α-HA) or with purified IgG from a control strain (Rol-6) and from transgenic lines expressing HA-CeOB1 and HA-CeOB2. The precipitates were either hybridized with nematode telomeric repeats [$(GCCTAA)_4$] or a probe against unrelated repeats (CeRep55). The input represents 10% of DNA used for ChIPs.

anti-HA antibodies (data not shown), and immunoprecipitations carried out as described (Verdun et al., 2005), using the intrachromosomal CeRep55 repeat as control. In two independent experiments anti-HA antibodies specifically precipitated nematode telomeric sequences from worms expressing HA tagged CeOB1 and CeOB2 (Figure 6B, left panel). No GCCTAA repeats were present in the precipitates from a control transgenic line (Rol-6), and in precipitations with pure IgG (Figure 6B, left panel). Conversely, anti-HA as well as purified IgG antibodies failed to precipitate the telomere unrelated CeRep55 repeats (Figure 6B, right panel), confirming that CeOB1 and CeOB2 do not bind to nontelomeric repeats.

Taken together, these findings suggest that CeOB1 and CeOB2 can bind to *C. elegans* telomeres in vivo.

## CeOB1 and CeOB2 Regulate Telomere Length

When we examined telomere length in the deletion mutants for CeOB1 (TM1400) and CeOB2 (TM1620) (deletion schematics in Figure 7A), telomere length was found to be altered. Telomeres in the wild-type N2 worms ranged from 2 to 8 kb (Cheung et al., 2004; Raices et al., 2005), while TM1400 and TM1620 telomeres were much longer (Figure 7B). To analyze the telomeres of strains lacking CeOB1 and CeOB2 we performed 2D gel electrophoresis and hybridization of the gels with probes specific for the telomeric G strand and the C strand under native and denaturing conditions. TM1400 mutants, lacking CeOB1, displayed extremely long telomeres (Figure 7C, second row, black arrows). The G overhangs signal appeared stronger, especially for shorter telomeres (Figure 7C, second row, native panels, blue arrow), suggesting that overhangs were elongated as well. Also, the intensity of the arc representing telomeric circles was strongly increased, indicating that circles accumulate when CeOB1 is missing, and circles were of larger molecular weight (Figure 7C, second row, denatured panels, red arrows). Deletion of CeOB2 led to a different phenotype. There were no changes in the overhang signal, but telomere length was much more heterogeneous, ranging from very short to very long, visible under native and denatured conditions (Figure 7C, third row, black arrows), and telomeric circles were also readily detectable under denatured conditions (Figure 7C, third row, red arrows). The heterogeneous nature of the telomeres in the CeOB2 deletion strain was reminiscent of the ALT phenotype, where telomeric restriction fragments ranges from extremely short to very long (Bryan et al., 1995; Dunham et al., 2000).

(F) Both CeOB1 and CeOB2 generate super-shifted species. Radioactively labeled $(GCCTAA)_3$ and $(TTAGGC)_3$ oligonucleotides are indicated. No antibody (-), purified IgG, or anti-His antibodies were added as indicated. Asterisks indicate the resulting bands.

(G) Competition assays were performed in the presence of a 1-, 10-, and 100-fold excess of unlabeled $(TTAGGC)_3$ and unrelated (NR) oligos. NP lanes contain no protein and (-) lanes contain no unlabeled oligonucleotides. Free oligos are indicated and asterisks show the bands resulting from addition of CeOB1.

(H) As in (F), except that CeOB2 binding was competed with a 5-, 100-, and 1000-fold excess of unlabeled $(GCCTAA)_3$ and unrelated (NR) oligos.

(I) Gel retardation assays testing whether His-CeOB1 or His-CeOB2 binding preferred a telomeric single-stranded terminus. His-CeOB1 (left panel) was either omitted from the reactions (- lanes) or incubated with oligonucleotides containing a $(TTAGGC)_3$ repeat at the 3′ end (NR-$(TTAGGC)_3$-3′) or the 5′ end (5′-$(TTAGGC)_3$-NR). His-CeOB2 was either omitted from the reactions (- lanes) or incubated with oligonucleotides containing a $(GCCTAA)_3$ repeat at the 3′ end (NR-$(GCCTAA)_3$-3′) or the 5′ end (5′-$(GCCTAA)_3$-NR). The signal resulting from the free oligos is indicated, and the asterisk indicates the band resulting from addition of the proteins.

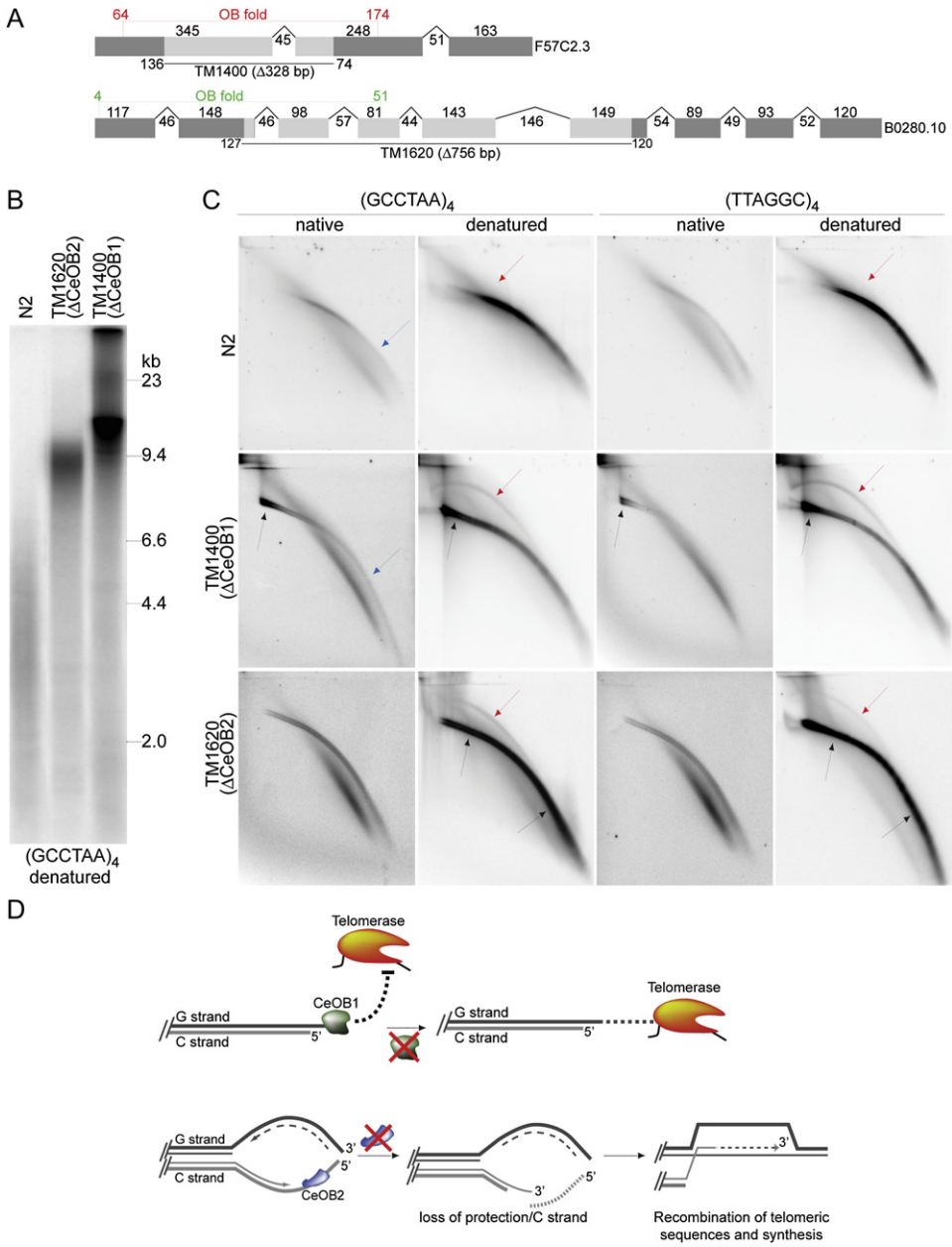


**Figure 7. Telomere Length Analysis upon Deletion of CeOB1 or CeOB2**

(A) Schematic of the deletions in *CeOB1* and *CeOB2*. Intron and exon structure of *CeOB1* (sequence name F57C2.3) and *CeOB2* (sequence name B0280.10), as well as their nucleotide length, has been indicated. The deleted area has been highlighted in light gray. The *CeOB1* deletion mutant is called TM1400, and the *CeOB2* deletion mutant TM1620. The OB folds of the proteins have been pointed out in red and green, with their starting and ending nucleotide number in the correlating exons.

(B) One-dimensional gel electrophoresis of *C. elegans* DNA isolated from wild-type strains (N2), a CeOB1 deletion strain (TM1400), or a CeOB2 deletion strain (TM1620). The gels have been hybridized with a radioactively labeled $(GCCTAA)_4$ oligonucleotide. Fragment size is indicted on the right.

(C) Native and denatured gel electrophoresis of *C. elegans* DNA isolated from wild-type strains (N2), a CeOB1 deletion strain (TM1400), or a CeOB2 deletion strain (TM1620). The gels have been hybridized with a radioactively labeled $(GCCTAA)_4$ oligonucleotide (left half) or a radioactively labeled $(TTAGGC)_4$ oligo. The black arrows indicate differences in telomere length, the blue arrow points at overhangs, and the red arrows points at the arc resulting from T circles as described in the text.

(D) Proposed models for mechanisms of CeOB1 and CeOB2 function.

In summary, we suggest that both nematode telomeric single-stranded binding proteins regulate telomere length. In our model we propose that CeOB1 influences telomerase mediated telomere elongation and the length of the 3′ G overhang, and CeOB2 suppresses recombination events at telomeres (Figure 7D).

## DISCUSSION

Single-stranded telomeric G tails with 3′ termini have been described in a variety of organisms and are central to chromosome end protection by distinguishing natural chromosome ends from double strand breaks.

Here, we show that telomeres in the nematode *C. elegans* carry 3′ G-rich overhangs and 5′ C-rich tails, a so far unique feature, which suggests that proteins that bind to single-stranded G-rich repeats are not sufficient for chromosome end protection. However at this point it is unclear whether these C overhangs are generated by 3′ to 5′ resection of the G-rich strand, or by incomplete replication.

We also demonstrate the presence of t loops and t circles at nematode telomeres, but the data presented here do not sufficiently explain if loops are the result of invasion of either G overhangs or C overhangs into double-stranded telomeric sequences. However, experiments in Figure 6 demonstrate that the base of the loops can be a substrate for both proteins, suggesting the presence of either single-stranded G-rich or single-stranded C-rich DNA there. An in vitro assay to test the invasion of a telomeric single strand of vertebrate sequence into double-stranded telomeric DNA showed no preference for polarity of the DNA (Verdun and Karlseder, 2006), allowing speculation that both, a 3′ G tail and a 5′ C tail can form loops by invasion.

Currently, no homologs of the proteins in the shelterin complex have been described in *C. elegans*. Homology searches with POT1 and TEBPα led to the identification of two OB fold containing factors, CeOB1 and CeOB2. The predicted 3D structure of CeOB1 aligned to the second OB fold of POT1, and CeOB2 to the first OB fold. In the *C. elegans* genome these proteins reside on different chromosomes (CeOB1 on chromosome II, and CeOB2 on chromosome III). Since *S. pombe*, *O. nova*, *A. thaliana*, *M. musculus* and *H. sapiens* all contain TEBPα like proteins with more than one OB fold, it is possible that in nematodes this protein split into two independent factors that fulfill different functions.

When we tested the binding properties of the two proteins to DNA, we found that CeOB1 binds to single-stranded G-rich telomeric DNA, whereas CeOB2 had a preference for C-rich telomeric single-stranded repeats. Therefore, we concluded that *C. elegans* evolved an OB fold dependent mechanism of protecting chromosome ends that terminate with either 3′ G tails or 5′ C tails. Since CeOB1 has homology to the second OB fold of POT1, and CeOB2 to the first OB fold, it remains to be tested whether the individual OB folds of POT1 or TEBPα can bind to C-rich telomeric single-stranded DNA.

These two proteins have different effects on telomere length. Deletion of CeOB1 led to the accumulation of extremely long telomeres, suggesting that CeOB1 plays a role in relaying control of telomere length to telomerase, as has been demonstrated for hPOT1 (Loayza and De Lange, 2003). This deletion also displayed longer telomeric G overhangs (Figure 7), a phenotype observed in mice without POT1b (Hockemeyer et al., 2006). Deletion of CeOB2 had no obvious effect on the telomeric G tail or C tail, but led to telomeres that were highly heterogeneous in length, reminiscent of an ALT phenotype.

We therefore suggest a model where CeOB1 and CeOB2 fill independent roles at telomeres. We propose that CeOB1 is a transducer of telomere length to telomerase by regulating the telomere specific reverse transcriptase at G overhangs. CeOB2 protects nematode specific telomeric single-stranded C-rich DNA from inappropriate recombination, which is apparent in a CeOB2 deletion strain that displays an ALT like phenotype. Although wild-type worms seem to rely mostly on telomerase dependent telomere maintenance, these mutants trigger an ALT like phenotype, suggesting that *C. elegans* could be an excellent model to study both major telomere maintenance pathways. Furthermore, the discovery that worms and ALT cells both contain single-stranded telomeric DNA, which does not seem to be associated with the telomeres, is intriguing. While only 3′ G-rich overhangs and G-rich ssDNA have been described in ALT cells, worms have both G-rich and C-rich ssDNA, in accordance with the presence of 3′ and 5′ overhang structures. This observation suggests that the ssDNA could be a by-product of overhang generation and processing. We are therefore confident that future experiments using the nematode model will allow the study of differences in telomere processing and replication that have been challenging to address in other model systems.

## EXPERIMENTAL PROCEDURES

### Strains

Worms were grown at 20°C and maintained as described (Brenner, 1974). The strains used are described in the Supplemental Data.

### Native and Denaturing Telomere Blots

Genomic DNA extraction from nematodes and telomere Southern blotting was performed as described (Raices et al., 2005). The nondenaturing hybridization assay to detect overhangs was carried out as described (Karlseder et al., 2002).

### Enzyme Treatments

For Bal-31 treatment DNA (100 μg) was treated with 20U of Bal-31 exonuclease (New England Biolabs) at 30°C in 500 μl of 1X Bal-31 buffer. Reactions were stopped with the addition of EGTA (25mM final concentration) at 0, 5, 10, 20, 30, 40, 60, and 120 min.

For Mung Bean Nuclease treatments, DNA (60 μg) was treated with 10U of Mung Bean Nuclease (New England Biolabs) at 30°C in 200 μl of 1× Mung Bean buffer. Reactions were stopped at 0, 10, 30 and 60 min. For ExoI and $RecJ_f$ treatments *C. elegans* DNA (2.5 −10 μg) was treated overnight with 100U of Exo I (United States Biochemicals) or 3000U of $RecJ_f$ (New England Biolabs). Samples were incubated at 37°C in 500 μl of 1X Exo I buffer or $RecJ_f$ buffer.

### Two-Dimensional Gel Electrophoresis

2D telomere blots were performed as described previously (Cesare and Griffith, 2004). For details, see Supplemental Data.

### Nuclei Preparation and DNA Purification for EM Analysis

Preparation of *C. elegans* wild-type CC2 embryos and isolation of nuclei was performed as previously described (Hope, 1999). For details, see Supplemental Data.

### Electron Microscopy

T loops and t circles were visualized by surface spreading of telomeric fractions from size exclusion chromatography on a denatured protein film as described previously (Griffith et al., 1999). For details, see Supplemental Data.

### Single Telomere Length Analysis

Genomic DNA was diluted to a 20 ng/μl concentration. A mix of 20 ng of DNA and 1 μl of 10 μM oligo (telorette) in a 2 μl volume was incubated at 60°C for

10 min. Ligation and PCR was carried out as described (Cheung et al., 2004). For details, and oligonucleotide sequences see Supplemental Data.

### Sequence Alignments and 3D Models

*C. elegans* candidate proteins were identified by searching for putative OB fold containing proteins with similarity to hPOT1 and POT1 homologs in the *C. elegans* genome database (http://www.wormbase.org). The proteins identified were analyzed using position-specific iterated (PSI)-BLAST searches of the nonredundant protein database (Altschul et al., 1997; Eddy, 1998). For details, see Supplemental Data.

### Protein Expression and Purification

CeOB1 and CeOB2 were cloned in a GATEWAY-modified pET28 vector carrying an N-terminal 9-His tag. The constructs were expressed in *E. coli* BL21 (DE3). For details, see Supplemental Data.

### Electrophoretic Mobility Shift Assays

Binding reactions were performed in 20 mM HEPES (pH 7.8), 25 mM KCl, 1.25 mM MgCl2, 1 mM DTT, 10 ng/μl tRNA, and 10% glycerol. DNA oligomers were 5′ end-labeled with [$^{32}$P] dATP by T4 polynucleotide kinase (New England Biolabs) and separated from unincorporated activity using an G-25 illustra Microspin Column (GE Healthcare). For the direct binding assays, a 50 nM final concentration purified proteins, similar to those reported (Wang et al., 2007) and radiolabeled oligomers (10 nM final concentration) were added sequentially to a 10 μl reaction, incubated 5 min at 25°C and electrophoresed through a 6% (w/v) nondenaturing polyacrylamide gel in 1X TBE at 12 V/cm. Gels were dried at 60°C for an hour and exposed to PhosphorImager screens. For CeOB2, all binding reactions were in the 50 mM KCl. When increasing amounts of His-CeOB1 or His-CeOB2 were used, the final concentrations were 25–50–100 nM.

For competition assays, proteins were incubated with a 1-, 5-, 10-, 100-, or 1000-fold excess of unlabeled competitors together with the radiolabeled oligomer 5 min at 25°C. For the supershift assays, the proteins were preincubated with for 5 min at 25°C with of 100 ng of the Monoclonal Anti-polyHis Antibody H1029 (Sigma) before the addition of the radiolabeled oligomer, and 5′ more after that. A similar amount of control normal rabbit IgG sc2027 (Santa Cruz) was used as a control. The oligomers used in this study are described in the Supplemental Data.

### $K_D$ measurement

The equilibrium dissociation constants ($K_D$) for CeOB1 and CeOB2 were determined by quantitative analysis of mobility shift assays as described (Travers and Buckle, 2000). Fore details see Supplemental Data.

### Generation of HA-Tagged CeOB1 and CeOB2 Constructs

*CeOB1* and *CeOB2* cDNAs were amplified by PCR and inserted in a modified version of the pPD95.77 vector (Fire Lab Vector Kit) that lacks the GFP marker. The hemagglutinin (HA) sequence was added to the PCR primers. The products generated were digested with BsmI and XmaI and cloned in the modified vector downstream the pha-4 promoter (Panowski et al., 2007) and upstream the UNC-54 3′ UTR. For sequences see Supplemental Data.

### Generation of Transgenic Lines

For the generation of transgenic animals, plasmid DNA containing the different constructs of interest were mixed at 75 μg/ml and pRF4 (*rol-6*) construct (Mello et al., 1991) were microinjected into the gonads of adult hermaphrodite animals N2 worms by using standard methods (Mello et al., 1991). Transgenic F1 progeny were selected on the basis of roller phenotype. Individual transgenic F2 animals were isolated to establish independent lines.

Expression of the tagged proteins was confirmed by Western blot using a monoclonal anti-HA antibody (HA.11, Covance). Wild-type N2 worms and a strain carrying the rol-6 marker alone were used as controls.

### Chromatin Immunoprecipitations

ChIPs were performed as described previously (Verdun et al., 2005) with minor variations. For detail see Supplemental Data.

## SUPPLEMENTAL DATA

Supplemental Data include three figures, four tables, Supplemental Experimental Procedures, and Supplemental References and can be found with this article online at http://www.cell.com/cgi/content/full/132/5/745/DC1/.

## ACKNOWLEDGMENTS

We thank E. Mandell from V. Lundblad's laboratory for advice and assistance with structure predictions and analysis; V. Lundblad and members of the Karlseder laboratory for critical comments on the manuscript; Z. Liu from A. Dillin's lab for generating transgenic worms; and M. D'Angelo from M. Hetzer's laboratory for help with protein expression. J.D.G. and J.K. acknowledge the National Institutes of Health (NIH) for funding (grants GM31819 and ES13773 to J.D.G. and GM06525 and AG025837 to J.K.). A.D. acknowledges the Ellison Medical Foundation for support. R.V. is a Leukemia and Lymphoma Society Fellow.

Received: August 9, 2007
Revised: November 21, 2007
Accepted: December 15, 2007
Published: March 6, 2008

## REFERENCES

Altschul, S.F., Madden, T.L., Schaffer, A.A., Zhang, J., Zhang, Z., Miller, W., and Lipman, D.J. (1997). Gapped BLAST and PSI-BLAST: A new generation of protein database search programs. Nucleic Acids Res. *25*, 3389–3402.

Anderson, E.M., Halsey, W.A., and Wuttke, D.S. (2002). Delineation of the high-affinity single-stranded telomeric DNA-binding domain of *Saccharomyces cerevisiae* Cdc13. Nucleic Acids Res. *30*, 4305–4313.

Baumann, P., and Cech, T.R. (2001). Pot1, the putative telomere end-binding protein in fission yeast and humans. Science *292*, 1171–1175.

Bianchi, A., Negrini, S., and Shore, D. (2004). Delivery of yeast telomerase to a DNA break depends on the recruitment functions of Cdc13 and Est1. Mol. Cell *16*, 139–146.

Booth, C., Griffith, E., Brady, G., and Lydall, D. (2001). Quantitative amplification of single-stranded DNA (QAOS) demonstrates that *cdc13–1* mutants generate ssDNA in a telomere to centromere direction. Nucleic Acids Res. *21*, 4414–4422.

Brenner, S. (1974). The genetics of *Caenorhabditis elegans*. Genetics *77*, 71–94.

Bryan, T.M., Englezou, A., Gupta, J., Bacchetti, S., and Reddel, R.R. (1995). Telomere elongation in immortal human cells without detectable telomerase activity. EMBO J. *14*, 4240–4248.

Cesare, A.J., and Griffith, J.D. (2004). Telomeric DNA in ALT cells is characterized by free telomeric circles and heterogeneous t-loops. Mol. Cell. Biol. *24*, 9948–9957.

Chai, W., Du, Q., Shay, J.W., and Wright, W.E. (2006). Human telomeres have different overhang sizes at leading versus lagging strands. Mol. Cell *21*, 427–435.

Chandra, A., Hughes, T.R., Nugent, C.I., and Lundblad, V. (2001). Cdc13 both positively and negatively regulates telomere replication. Genes Dev. *15*, 404–414.

Cheung, I., Schertzer, M., Baross, A., Rose, A.M., Lansdorp, P.M., and Baird, D.M. (2004). Strain-specific telomere length revealed by single telomere length analysis in *Caenorhabditis elegans*. Nucleic Acids Res. *32*, 3383–3391.

de Lange, T. (2004). T-loops and the origin of telomeres. Nat. Rev. Mol. Cell Biol. *5*, 323–329.

de Lange, T. (2005). Shelterin: The protein complex that shapes and safeguards human telomeres. Genes Dev. *19*, 2100–2110.

Diede, S.J., and Gottschling, D.E. (1999). Telomerase-mediated telomere addition in vivo requires DNA primase and DNA polymerases alpha and delta. Cell *99*, 723–733.

Dionne, I., and Wellinger, R.J. (1996). Cell cycle-regulated generation of single-stranded G-rich DNA in the absence of telomerase. Proc. Natl. Acad. Sci. USA *93*, 13902–13907.

Dunham, M.A., Neumann, A.A., Fasching, C.L., and Reddel, R.R. (2000). Telomere maintenance by recombination in human cells. Nat. Genet. *26*, 447–450.

Eddy, S.R. (1998). Profile hidden Markov models. Bioinformatics *14*, 755–763.

Fan, X., and Price, C.M. (1997). Coordinate regulation of G- and C strand length during new telomere synthesis. Mol. Biol. Cell *8*, 2145–2155.

Garvik, B., Carson, M., and Hartwell, L. (1995). Single-stranded DNA arising at telomeres in *cdc13* mutants may constitute a specific signal for the *RAD9* checkpoint. Mol. Cell. Biol. *15*, 6128–6138.

Grandin, N., Damon, C., and Charbonneau, M. (2001). Cdc13 prevents telomere uncapping and Rad50-dependent homologous recombination. EMBO J. *20*, 6127–6139.

Grandin, N., Reed, S.I., and Charbonneau, M. (1997). Stn1, a new *Saccharomyces cerevisiae* protein, is implicated in telomere size regulation in association with Cdc13. Genes Dev. *11*, 512–527.

Gray, H.B., Jr., Ostrander, D.A., Hodnett, J.L., Legerski, R.J., and Robberson, D.L. (1975). Extracellular nucleases of Pseudomonas BAL 31. I. Characterization of single strand-specific deoxyriboendonuclease and double-strand deoxyriboexonuclease activities. Nucleic Acids Res. *2*, 1459–1492.

Griffith, J.D., Comeau, L., Rosenfield, S., Stansel, R.M., Bianchi, A., Moss, H., and de Lange, T. (1999). Mammalian telomeres end in a large duplex loop. Cell *97*, 503–514.

Gubler, U. (1987). Second-strand cDNA synthesis: mRNA fragments as primers. Methods Enzymol. *152*, 330–335.

Hemann, M.T., and Greider, C.W. (1999). G-strand overhangs on telomeres in telomerase-deficient mouse cells. Nucleic Acids Res. *27*, 3964–3969.

Hockemeyer, D., Daniels, J.P., Takai, H., and de Lange, T. (2006). Recent expansion of the telomeric complex in rodents: Two distinct POT1 proteins protect mouse telomeres. Cell *126*, 63–77.

Hope, I. (1999). *C. elegans*: A Practical Approach (Oxford: Oxford University Press).

Jacob, N.K., Kirk, K.E., and Price, C.M. (2003). Generation of telomeric G strand overhangs involves both G and C strand cleavage. Mol. Cell *11*, 1021–1032.

Jacob, N.K., Skopp, R., and Price, C.M. (2001). G-overhang dynamics at Tetrahymena telomeres. EMBO J. *20*, 4299–4308.

Karlseder, J., Smogorzewska, A., and de Lange, T. (2002). Senescence induced by altered telomere state, not telomere loss. Science *295*, 2446–2449.

Lei, M., Baumann, P., and Cech, T.R. (2002). Cooperative binding of single-stranded telomeric DNA by the Pot1 protein of *Schizosaccharomyces pombe*. Biochemistry *41*, 14560–14568.

Loayza, D., and De Lange, T. (2003). POT1 as a terminal transducer of TRF1 telomere length control. Nature *423*, 1013–1018.

Lovett, S.T., and Kolodner, R.D. (1989). Identification and purification of a single-stranded-DNA-specific exonuclease encoded by the recJ gene of *Escherichia coli*. Proc. Natl. Acad. Sci. USA *86*, 2627–2631.

Makarov, V.L., Hirose, Y., and Langmore, J.P. (1997). Long G tails at both ends of human chromosomes suggest a C strand degradation mechanism for telomere shortening. Cell *88*, 657–666.

McElligott, R., and Wellinger, R.J. (1997). The terminal DNA structure of mammalian chromosomes. EMBO J. *16*, 3705–3714.

Meier, B., Clejan, I., Liu, Y., Lowden, M., Gartner, A., Hodgkin, J., and Ahmed, S. (2006). trt-1 is the *Caenorhabditis elegans* catalytic subunit of telomerase. PLoS Genet. *2*, e18. 10.1371/journal.pgen.0020018.eor.

Mello, C.C., Kramer, J.M., Stinchcomb, D., and Ambros, V. (1991). Efficient gene transfer in *C. elegans*: Extrachromosomal maintenance and integration of transforming sequences. EMBO J. *10*, 3959–3970.

Nakamura, M., Nabetani, A., Mizuno, T., Hanaoka, F., and Ishikawa, F. (2005). Alterations of DNA and chromatin structures at telomeres and genetic instability in mouse cells defective in DNA polymerase alpha. Mol. Cell. Biol. *25*, 11073–11088.

Nikaido, R., Haruyama, T., Watanabe, Y., Iwata, H., Iida, M., Sugimura, H., Yamada, N., and Ishikawa, F. (1999). Presence of telomeric G-strand tails in the telomerase catalytic subunit TERT knockout mice. Genes Cells *4*, 563–572.

Nugent, C.I., Hughes, T.R., Lue, N.F., and Lundblad, V. (1996). Cdc13p: A single-strand telomeric DNA-binding protein with a dual role in yeast telomere maintenance. Science *274*, 249–252.

Panowski, S.H., Wolff, S., Aguilaniu, H., Durieux, J., and Dillin, A. (2007). PHA-4/Foxa mediates diet-restriction-induced longevity of *C. elegans*. Nature *447*, 550–555.

Pennock, E., Buckley, K., and Lundblad, V. (2001). Cdc13 delivers separate complexes to the telomere for end protection and replication. Cell *104*, 387–396.

Raices, M., Maruyama, H., Dillin, A., and Karlseder, J. (2005). Uncoupling of longevity and telomere length in *C. elegans*. PLoS Genet *1*, e30. 10.1371/journal.pgen.0010030.

Riha, K., McKnight, T.D., Fajkus, J., Vyskot, B., and Shippen, D.E. (2000). Analysis of the G-overhang structures on plant telomeres: evidence for two distinct telomere architectures. Plant J. *23*, 633–641.

Sfeir, A.J., Chai, W., Shay, J.W., and Wright, W.E. (2005). Telomere-end processing the terminal nucleotides of human chromosomes. Mol. Cell *18*, 131–138.

Theobald, D.L., and Wuttke, D.S. (2004). Prediction of multiple tandem OB-fold domains in telomere end-binding proteins Pot1 and Cdc13. Structure *12*, 1877–1879.

Travers, A.A., and Buckle, M. (2000). DNA-Protein Interactions: A Practical Approach (Oxford: Oxford University Press).

Verdun, R.E., Crabbe, L., Haggblom, C., and Karlseder, J. (2005). Functional Human Telomeres Are Recognized as DNA Damage in G2 of the Cell Cycle. Mol. Cell *20*, 551–561.

Verdun, R.E., and Karlseder, J. (2006). The DNA damage machinery and homologous recombination pathway act consecutively to protect human telomeres. Cell *127*, 709–720.

Wang, F., Podell, E.R., Zaug, A.J., Yang, Y., Baciu, P., Cech, T.R., and Lei, M. (2007). The POT1–TPP1 telomere complex is a telomerase processivity factor. Nature *445*, 506–510.

Wang, R.C., Smogorzewska, A., and de Lange, T. (2004). Homologous recombination generates T-loop-sized deletions at human telomeres. Cell *119*, 355–368.

Wellinger, R.J., Ethier, K., Labrecque, P., and Zakian, V.A. (1996). Evidence for a new step in telomere maintenance. Cell *85*, 423–433.

Wellinger, R.J., Wolf, A.J., and Zakian, V.A. (1993). *Saccharomyces* telomeres acquire single-strand TG1–3 tails late in S phase. Cell *72*, 51–60.

Wright, W.E., Tesmer, V.M., Huffman, K.E., Levene, S.D., and Shay, J.W. (1997). Normal human chromosomes have long G-rich telomeric overhangs at one end. Genes Dev. *11*, 2801–2809.